Tetrahedron 67 (2011) 1696–1702

Contents lists available at ScienceDirect

Tetrahedron

journal homepage: www.elsevier.com/locate/tet

Blue light-emitting and electron-transporting materials based on dialkyl-functionlized anthracene imidazophenanthrolines

Jiann-Fong Lee [a], Yung-Chung Chen [b], Jiann-T'suen Lin [b], Chung-Chih Wu [c], Chien-Yu Chen [c], Chi-An Dai [d], Chi-Yang Chao [a], Hsuen-Li Chen [a,*], Wen-Bin Liau [a,*]

[a] Department of Materials Science and Engineering, National Taiwan University, Taipei 106, Taiwan
[b] Institute of Chemistry, Academia Sinica, Taipei 115, Taiwan
[c] Graduate Institute of Photonics and Optoelectronics, National Taiwan University, Taipei 106, Taiwan
[d] Department of Chemical Engineering, National Taiwan University, Taipei 106, Taiwan

ARTICLE INFO

Article history:
Received 21 May 2010
Received in revised form 14 December 2010
Accepted 21 December 2010
Available online 25 December 2010

Keywords:
Blue light-emitting dioide
Imidazophenanthroline
Electron-transporting material

ABSTRACT

Two novel blue light-emitting materials based on bis(*tert*-butyl)anthracenyl-imidazophenanthrolines (**BAIP**s) have been synthesized and extensively characterized. Both materials exhibited a non-aggregate feature with high fluorescent quantum efficiency and excellent thermal stability. They can serve both as emissive and electron-transporting materials used in electroluminescence (EL) device for blue emission with high luminescence and external quantum efficiency. This study demonstrates that they are potentially useful for a wide range of applications in EL technology.

1. Introduction

Organic electroluminescent materials continue to be of considerable worldwide research interest.[1,2] Many organic compounds, both small molecules and polymeric materials, have been developed and tested for use in organic light-emitting devices (OLEDs). The use of small molecules provides benefits including unambiguous structural identification, easy synthesis, high purity, and good solubility. The hole mobility of small organic molecules is generally orders of magnitude higher than their electron mobility such that most of small organic molecules are used as a hole transporting material (HTMs). However, tris(8-hydroxyquinoline) aluminum (Alq_3) developed by Tang and Van-Slyke at Kodak in the late 80s exhibits an excellent emission in the green light region and good electron-transporting property.[3] Since then, it has been extensively investigated in various OLED device structures as the principal electron-transporting material (ETM).

The use of Alq_3 as a host material for other fluorophores has also been demonstrated.[4–6] Phosphorescent materials attract overwhelming popularity in recent years as they are expected to perform better than fluorescent materials in OLEDs.[7–9] However, blue-emitting fluorescent materials will continue to play an important role in the near future because the synthesis of a true blue-emitting as well as stable phosphor is still challenging. Therefore, it should be useful to develop other highly efficient blue-emitting fluorescent materials that are also capable of electron-transporting as a replacement for Alq_3. Compared to green-emitting Alq_3, a blue-emitting host will likely have a larger triplet energy for phosphorescent dopants with larger triplet energy.

Anthracene and phenanthroline derivatives are important blue light-emitting and charge-transporting materials.[10–12] Effective combination of two individual benefits will be interesting topics. Mondal and several other research groups have demonstrated that some arylimidazo-fused phenanthrolines (AIPs) derivatives exhibited fast electron transport/injection and bright blue light-emitting features.[13–15] Extensive π–π stacking between neighboring imidazophenanthrolines (IPs) and aromatic units in AIPs resulted in their rigidity nature and fast electron mobility in the solid state. Nevertheless, the strong aggregation tendency of AIPs not only leads to the red shifting of their emission spectra, but also results in the deterioration of the device or solid-state optical performance.[13–19] We therefore set out to synthesize a no-aggregation congeners of AIPs via the incorporation of two *tert*-butyl groups acid-catalyzed alkylation at 2 and 6 positions of the anthracene. Such approach, i.e., aggregation suppression by increasing the steric congestion, has exhibited the optical gains herein and the similar concept has been elucidated in several reports.[20–22] Incidentally,

* Corresponding authors. Tel.: +886 2 33661318; fax: +886 2 23634562 (W.B.L.); tel.: +886 2 33663240; fax: +886 2 23634562 (H.L.C.); e-mail addresses: hsuenlichen@ntu.edu.tw (H.-L. Chen), wbliau@ntu.edu.tw (W.-B. Liau).

0040-4020/$ – see front matter © 2010 Elsevier Ltd. All rights reserved.
doi:10.1016/j.tet.2010.12.059

there are only a few instances of AIPs that function both as emitting as well as charge-transporting materials.[13–15] We expected these two **BAIP**s to serve as emitting and electron-transporting materials and also with high thermal stability.

2. Results and discussion

2.1. Scope of reaction

Scheme 1 outlines the synthetic protocol. 2,6-Di-*tert*-butylanthracene **4** can be facilely prepared in large laboratory scale by a known method.[23] The treatment of **4** with 1 equiv of *N*-bromosuccinimide (NBS) in dichloromethane afforded 2,6-di-*tert*-butyl-9-halide anthracene (**5**). A subsequent reaction of **5** with anhydrous *N*,*N*-dimethyl formamide (DMF) in THF led to the formation of 2,6-di-*tert*-butyl-9-formylanthracene (**6**). Compound **6** was then allowed to react with *ortho*-phenanthrolines-5,6-diketone and ammonia to give the parent compound of **1** and **2**, 2-(2,6-di-*tert*-butylanthracen-9-yl)-1*H*-imidazo[4,5-*f*][1,10] phenanthroline (**BAIP**). The desired products, **1** and **2**, can then be obtained by methylation and cyanylation of **BAIP**, respectively. The structure of the final products **1** and **2** is shown in Scheme 1. The thermal properties of the compounds were measured by using different scanning calorimetry (DSC). No phase transition was observed in the high temperature range tested (ranging from room temperature to 300 °C).

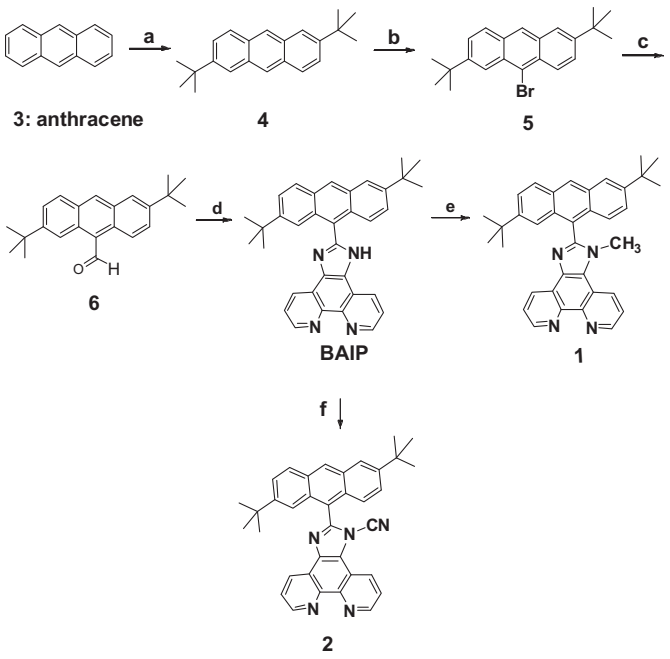

Scheme 1. Synthetic procedures for **BAIP** derived compounds (a) *tert*-butyl alcohol, TFA, reflux for 16 h (85%); (b) NBS and CH_2Cl_2, at 0 °C at rt for 1 h (46%); (c) *n*-BuLi, THF, and DMF at −78 °C for 2 h (45%); (d) NH_4OAc, phenanthracenedione, and HOAc, reflux for 2 h (50%); (e) NaH, CH_3I, and DMF at rt for overnight (45%); (f) NaH, BrCN, and DMF at rt for overnight (67%).

2.2. Photophysical property studies

The UV–vis absorption and emission spectra for **BAIP**, **1**, **2**, and 2-(anthracen-9-yl)-1-methyl-1*H*-imidazo[4,5-*f*][1,10](phenanthroline) (**MAIP**)[15] are shown in Fig. 1. The absorption profiles for the three **BAIP** derivatives are similar and consistent with the pattern reported previously for the absorption of other AIP analogs. The absorption profile of the compounds is basically the superposition of 2,6-di-*tert*-butylanthracene and imidazophenanthroline units.[14,15]

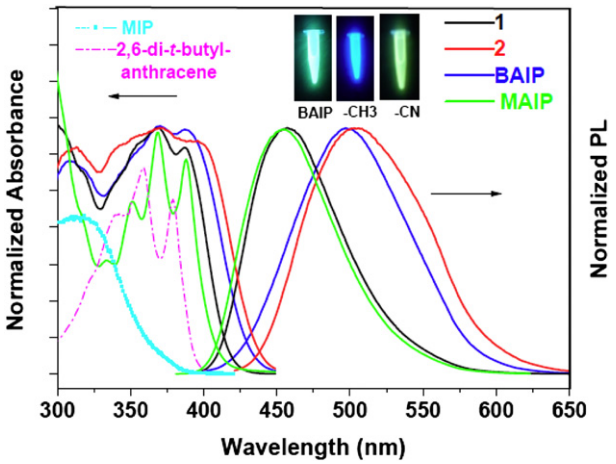

Fig. 1. UV–vis absorption (left) and photoluminescence (right) spectra of **1** (black line), **2** (red line), **BAIP** (blue line), and **MAIP** (green line) in dichloromethane. The absorption of **MIP** (1-methyl-1*H*-imidazo[4,5-*f*][1,10]phenanthroline, cyan line) and 2,6-di-*tert*-butylanthracene (magenta line) are recorded by the constituted moieties of **BAIP**s. Inset shows the photographs of blue emission from the solution of **1**, **2**, and **BAIP** upon excitation with a hand-held UV lamp. (For interpretation of the references to colour in this figure legend, the reader is referred to the web version of this article).

The dilute solution of **BAIP**s in dichloromethane (ca. 4×10^{-5} M) exhibits a blue emission between 456 and 503 nm (Table 1), and the quantum yield reaches 0.78 for **1** and 0.47 for **2**, with the full widths at half maximum (FWHM) of ca. 80 nm for **1** and 110 nm for **2** (Fig. 1). The structureless emissions of **BAIP**s are attributed to the fluorescence of imidazophenanthroline due to efficient energy transfer from the 2,6-di-*tert*-butylanthracene to the imidazophenanthroline unit.[14] In dilute state, **MAIP** has very similar absorption and emission spectra as **1**, indicating that the *tert*-butyl group introduces only minimal perturbation. Surprisingly, the replacement of the methyl substituent in **1** by a cyano-group to form compound **2** resulted in a dramatic reduction of the quantum yields of the imidazophenanthroline derivative, which is due to the presence of the strong intermolecular interaction induced by polar nature of the cyano entity.[24] The emission maximum of **2** in the film state was blue shifted by 15 nm compared to that in dilute solution, i.e., from 503 nm of the solution state to 488 nm of the film state. The emission maximums of **BAIP** in the film states were also blue shifted by 34 nm compared to that in dilute solution. In comparison, the film state emission of **MAIP** is red shifted by 49 nm (Table 1) compared to the solution state because of strong aggregation of the compound through π–π* interaction of anthracenyl units.[15] It is possible that the two *tert*-butyl groups effectively suppress similar π–π* interaction at the anthracenyl units in **BAIP** and **2**. The blue shift of **BAIP** and **2** may be due to H-type aggregation of imidazophenanthroline units, or less intermolecular interaction of the dyes in the film state compared to the interaction of the dye molecule with the solvent.[9]

2.3. Electrochemical studies and EL performance

Fig. 2 shows the CV plots of the **1** and **2**. Their oxidation peaks were 1.01 V for **1** and 1.12 V for **2**, respectively. The energy levels of the highest-occupied molecular orbital (HOMO) and the lowest-unoccupied molecular orbital (LUMO) are calculated from the onset oxidation [Eonset(Ox)] potentials with the formula expressed to $E_{HOMO}=-4.8-E_{onset}(Ox)$ (−4.8 V for SCE with respect to the zero vacuum level). The calculated data corresponding to their HOMO energy levels are −5.65 eV for **1** and −5.71 eV for **2**. The HOMO and LUMO levels suggest that compounds **1** and **2** may be capable of hole- and electron-transporting.

Table 1
Summary of optical absorption, photoluminescence (PL), quantum yield, electrochemical data, and thermal properties

Compound	$\lambda_{abs\ max}$[a] (nm)	Band gap[b] (eV)	PL λ_{max}[a,c] sol/film/$\Delta\lambda_{max}$ (nm)	Φ[d] sol/film	LUMO/HOMO (eV)[e]	T_g[f]/(°C)	T_m[f]/(°C)
BAIP	364, 385	2.97	496/462/−34	0.69/0.150	−2.71/−5.68	ND[g]	ND
1	363, 385	3.00	456/460/+4	0.78/0.523	−2.65/−5.65	ND	ND
2	363, 389	2.95	503/488/−15	0.47/0.352	−2.76/−5.71	ND	ND
MAIP[15]	351, 369, 387	2.95	452/501/+49	0.75/0.250[h]	−2.65/−5.60	—[i]	362

[a] In dichloromethane (ca. 4.0×10^{-5} M).
[b] From absorption onset values.
[c] $\lambda_{ex(sol)}$=370 nm and $\lambda_{ex(film)}$=370 nm.
[d] For dichloromethane solutions and vacuum-deposited films (1000 Å) by using the referenced **MAIP** in CH_2Cl_2 had a quantum yield of 0.75 Ref. 15 and films by integrating sphere method.
[e] HOMO values were calculated from oxidation potentials, while LUMO values were calculated by subtracting band gap values from their HOMO values.
[f] Baseline shift in the second heating DSC traces with a heating rate of 10 °C/min in nitrogen atmosphere.
[g] Not detectable.
[h] From single layer device.
[i] No data.

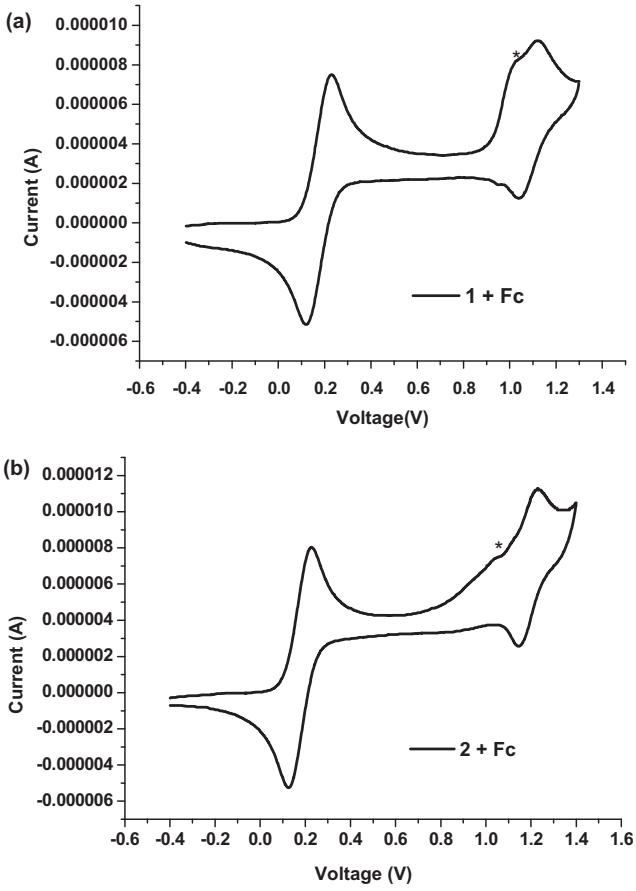

Fig. 2. CV plots of **1** (a) and **2** (b) (scan rate: 10 m V^{-1}, solvent: CH_2Cl_2). *The peaks with asterisk are due to impurity.

Herein, we have found that the compound **1** has similar HOMO level with **MAIP**,[15] indicating that the *tert*-butyl units have negligible electronic effect on the anthracene. The LUMO values for compounds **1** and **2** were calculated based on their respective band gap energy obtained from the tail-end of their UV–vis absorptions and the HOMO values (Table 1). Based on the HOMO and LUMO levels, these compounds are expected to have reasonable electron and hole mobility.

Fig. 3 shows the configuration and the HOMO, LUMO alignments in EL devices for **1** (device A) and for **2** (device B). The configuration of the multilayer device is shown as followed: (A) ITO/NPB (30 nm)/**1** (10 nm)/TPBI (40 nm)/LiF (1 nm)/Al (120 nm); (B) ITO/NPB (30 nm)/**2** (10 nm)/TPBI (40 nm)/LiF (1 nm)/Al (120 nm). For both

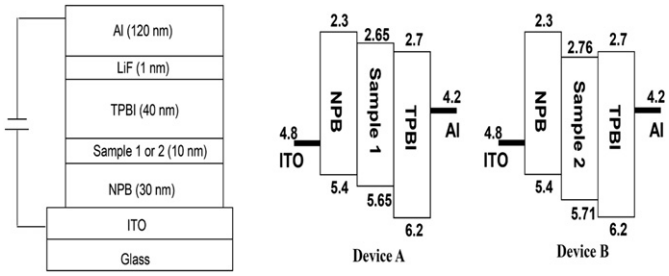

Fig. 3. The configurations of the EL devices and the energy levels of the compounds utilized in the device A and B.

types of the devices, 4,4-bis[*N*-(1-naphthyl)-*N*-phenylamino]biphenyl (NPB) was used as the hole-transporting layer, and 1,3,5-tris (*N*-phenyl benzimidazol-2-yl)-benzene (TPBI) was used as the electron-transporting materials.

Fig. 4 illustrates the EL spectra of the devices A and B at a driving voltage of 5.0 V. The EL spectra of both devices are almost identical to the PL spectra of **1** and **2** thin films. This result clearly shows that the emission in both devices A (λ_{em}=460 nm) and B (λ_{em}=488 nm) is solely from compounds **1** and **2**, respectively. The FWHM values of the EL spectra were estimated to be around 74 nm for the device A and 110 nm for the device B. The CIE (Commission Internationale del'Eclairage) color coordinates of devices A and B are (0.16, 0.18) and (0.23, 0.38) (Table 2), respectively. In addition, all the device performance data are presented in Table 2. The luminescence–voltage–current

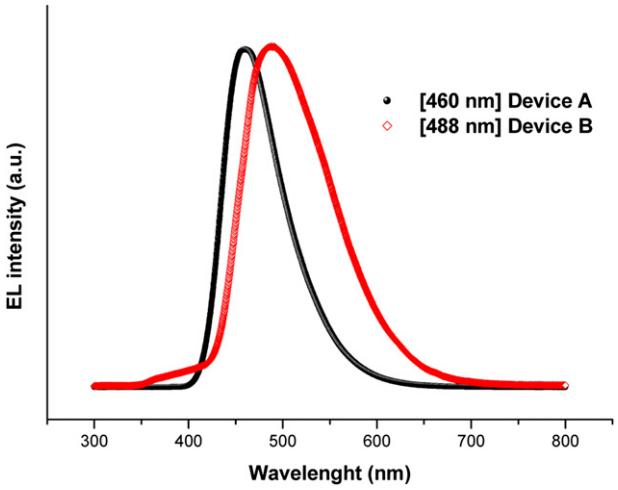

Fig. 4. EL spectra of the devices A and B at a driving voltage of 5.0 V.

density and EQE–current density–power are shown in Figs. 5a,b and 6a,b, respectively. Both types of devices have low turn-on voltages: 5.0 V for the device A and 4.0 V for the device B. This implies that there is no large energy barrier at the interface of the two devices. Device A exhibits a luminescence of 981 cd/m^2 at 9.5 V, the maximum power efficiency of 0.43 lm/W and the maximum external quantum efficiency of 0.57%. Device B displays the maximum brightness of 824 cd/m^2 at 10 V, the maximum power efficiency of 0.42 lm/W, and the maximum external quantum efficiency of 0.38%. In general, device A exhibited a much better EL performance compared with device B.

Table 2
EL data for device A and B

Device	V_{on}[a]	η_{ex}[b]/V	η_p[c]	η_l[d]/V	λ_{max}	L_{max}[e]/V_d[f]	CIE (x, y)
A	5.0	0.565/6.04	0.426	0.817	460	981/9.5	0.16, 0.18
B	4.0	0.352/6.43	0.418	0.857	488	824/10	0.23, 0.38

[a] Turn-on voltage.
[b] External quantum efficiency (%),
[c] Power efficiency (lm/W), and
[d] Luminance efficiency (cd/A) were at 20 mA/cm^2.
[e] Maximum luminance achieved (cd/m^2).
[f] Driving voltage (V_d).

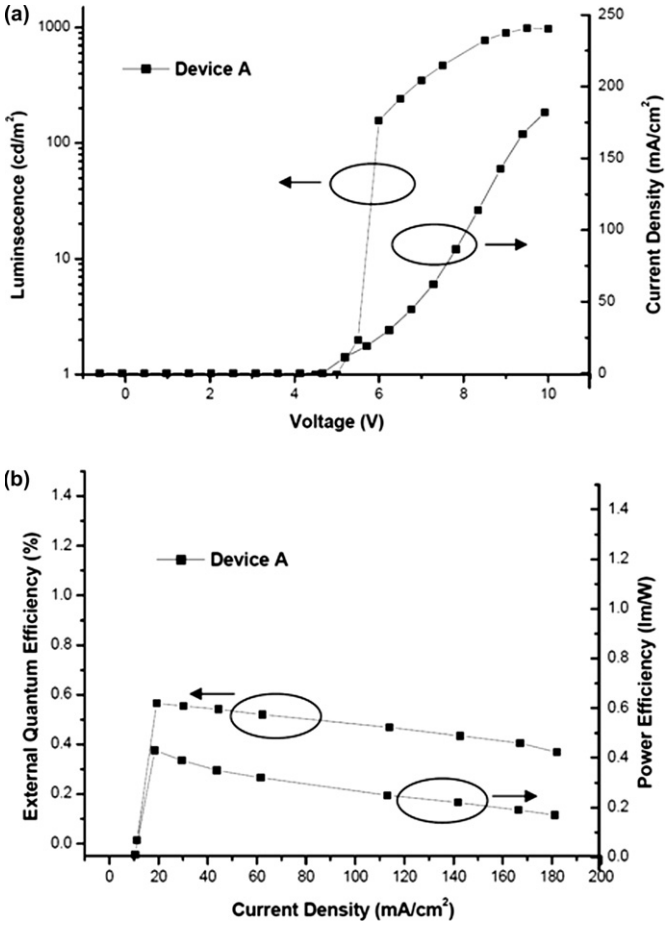

Fig. 5. The electro-optical characteristic of device A (a) Luminescence and current density as a function of voltage, and (b) EQE and power efficiency as a function of current density.

2.4. Charge mobility studies

To evaluate the performance of **1** as electron/hole transporting material, a time-of-flight (TOF) device was constructed to measure the electron and hole mobility. The absorption spectrum of **1** at

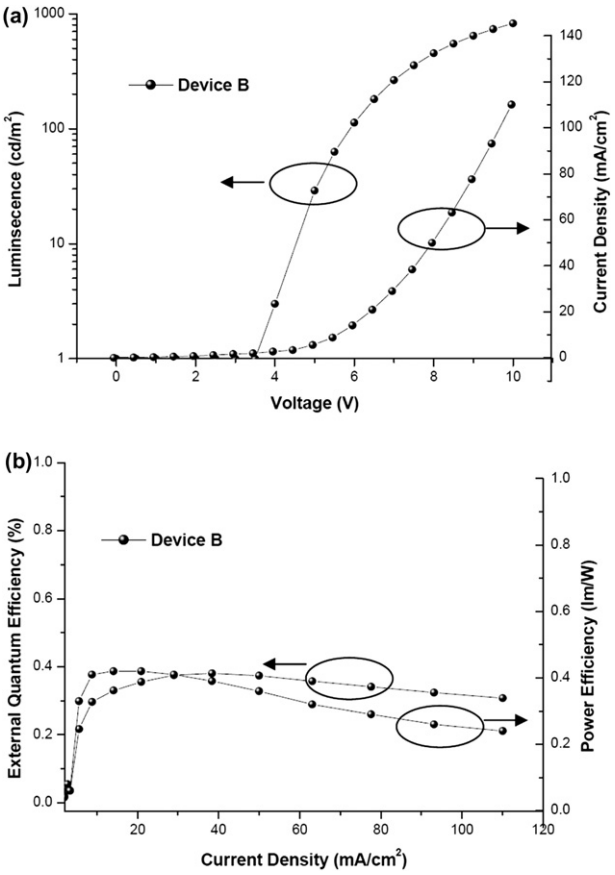

Fig. 6. The electro-optical characteristic of device B (a) Luminescence and current density as a function of voltage, and (b) EQE and power efficiency as a function of current density.

325–375 nm matches that of the frequency-tripled Nd:YAG laser (355 nm, 10 ns pulse width) systems used in this TOF measurements. Fig. 7(a) shows the representative TOF sample configuration of quartz substrate/Ag (30 nm)/**1** (2.36 μm)/Ag (160 nm). Both transients show a constant-current plateau followed by a rapid fall off, a clear signature of non-dispersive carrier transport. Using the carrier transit time t_T unambiguously evaluated from the intersection point of the asymptotes to the plateau and the tail sections in the double logarithmic representation of Fig. 7(b). Hole and electron mobility of **1** measured at room temperature are shown as a function of the square root of the electric field ($E^{1/2}$) in Fig. 7(c). Compound **1** has maximum electron mobility of 1.9×10^{-5} cm^2/Vs and hole mobility of 1.1×10^{-5} cm^2/Vs, respectively. The electron mobility of compound **1** is comparable with that of Alq_3.[25,26] The preliminary experimental data clearly indicated that compound **1** has excellent thermal stability and effective electron-transporting mobility. This together with the blue-emission characteristic renders the compound to be potentially useful for a wide range of applications in EL technology.

3. Conclusion

In summary, two bright thermally stable compounds based on bis(*tert*-butyl)anthracenyl-imidazo-phenanthrolines have been synthesized and characterized. Both compounds exhibit high fluorescent quantum yields both in solution and in the solid states. A triple-layered device was fabricated using both compounds **1** and **2** as the emitting fluorophore, TPBI, and NPB as the electron-transporting layer and the hole-transporting layer, respectively. The

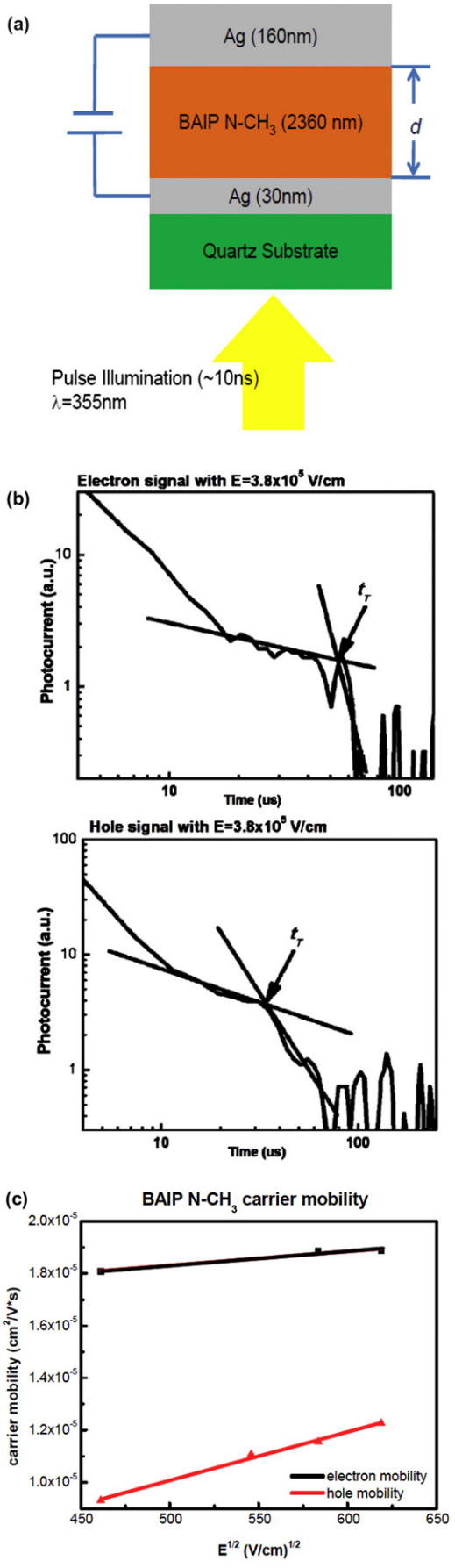

Fig. 7. Representative TOF transients (a) device configuration (b) TOF signals of **1** at $E=3.8\times10^5$ V/cm. (c) Hole and electron mobility versus $E^{1/2}$ for **1**.

blue-emitting device A exhibits luminescence of 981 cd/m^2 at 9.5 V, the maximum power efficiency of 0.43 lm/W, and the maximum external quantum efficiency of 0.57%. In addition, the electron mobility of the compound **1** is capable of electron-transporting as a replacement for Alq_3. More comprehensive studies on OLED applications of these new compounds will be pursued in the future.

4. Experimental

4.1. Instrumentation

Different scanning calorimetry (DSC) measurements were carried out using a Perkin–Elmer 7 series thermal analyzer at a heating rate of 10 °C/min from 30 to 300 °C. ^{1}H NMR and ^{13}C NMR spectra were recorded using a Bruker DMX-500 FT-NMR spectrometer. The chemical shifts were recorded in parts per million downfield from that of Me_4Si standard. FT-IR spectra were measured by using a Perkin–Elmer 1760-X FT-IR spectrometer. Mass spectra were recorded on Jeol JMS-D300 and FINNIGAN TSQ-46C mass spectrometers and HRMS was obtained with Jeol JMS-HX110 spectrometer. TLC was performed using Merck (Art. 5715) silica gel plates. TLC films were visualized under UV light (254 nm), after a treatment of iodine vapor, or a heating treatment followed by the exposure treatment of 5% phosphomolybdic acid in ethanol. Flash column chromatography was performed to purify all synthesized compounds using Merck (Art. 9385) 40–63 μm silica gel 60.

4.2. OLED fabrication and measurement

First, a prepatterned ITO substrate area was cleaned with acetone wash followed by methanol and acetone. Then, the triple-layer devices were prepared by vacuum deposition of 30 nm 4,4′-bis[*N*-(1-naphthyl)-*N*-phenylamino]biphenyl (NPB) as the hole-transport, 10 nm of the compounds **1** or **2** as the emitting layer, followed by 40 nm (1,3,5-tris(*N*-phenylbezimidazol-2-yl)benzene) as the electron-transport layer. Finally, a layer of LiF/Al (1 nm/120 nm) cathode was thermally evaporated as a cathode. The *I*–*V* curves were measured on a Keithley 2400 Source Meter in the ambient environment. The light intensity was measured with a Newport 1835 Optical Meter.

4.3. Charge mobility measurement

Charge transport in films was typically characterized in vacuum by applying the time-of-flight (TOF) transient photocurrent technique on quartz/Ag (30 nm)/organic sample (~μm)/Ag (150 nm) samples. Pulsed illumination (third harmonic of Nd:YAG laser, 355 nm, 10 ns) through the semitransparent electrode (Ag) induces photogeneration of a thin sheet of excess carriers. The sample thickness had been chosen to be much larger than the optical absorption depth of the excitation. Depending on the polarity of the applied bias, selected photogenerated carriers (holes or electrons) are swept across the sample with a transit time t_T. With the applied bias V and the sample thickness D, the applied electric field E is then V/D, and the carrier mobility is given by $\mu=D/(t_T\times E)=D^2/(V\times t_T)$.

4.4. Synthetic procedures and characterization of products

*4.4.1. (2,6-Di-tert-butylanthracene) (**4**).* Anthracene (10.0 g, 56.10 mmol), *tert*-butyl alcohol (16 mL, 168.30 mmol), and TFA (trifluoroacetic acid, 70 mL) were heated at reflux for 16 h. After cooling, the black crude mixture was treated with solid sodium bicarbonate. Water (150 mL) and hexane (150 mL) were added. The organic phase was separated and methylene chloride (CH_2Cl_2) was added to obtain a clear solution. The organic solvent was removed in vacuum and the residue was treated with hexane and

refrigerated. The white solid was filtered and washed with a small amount of cold hexane. The yield of crude **6** is 85% (12.3 g). ^{1}H NMR (500 MHz, $CDCl_3$) δ 1.45 (s, 18H), 7.55 (dd, J=8.9, 1.7 Hz, 2H), 7.87 (s, 2H), 7.93 (d, J=8.9 Hz, 1H), 8.33 (s, 2H).

*4.4.2. (9-Bromo-2,6-di-tert-butylanthracene) (**5**).* To a mixture of **4** (3.2 g, 11.0 mmol), NBS (1.96 g, 11.0 mmol) in anhydrous CH_2Cl_2 (50 mL) was added to react for 1 h at room temperature. The mixture was poured into a water bath and extracted with ethyl acetate. The ethyl acetate extract was sequentially washed with water, brine, and dried ($MgSO_4$) to filter out impurity and to give a crude product. Flash chromatography (ethyl acetate (EtOAc) /*n*-hexane=1:10) was then used to further purify the products followed by crystallization from ethyl acetate/*n*-hexane and evaporation to give **5** (1.6 g, 46%) as pale-yellow solid. ^{1}H NMR (500 MHz, $CDCl_3$) δ 1.46 (s, 9H), 1.49 (s, 9H), 7.58 (dd, J=9.0, 1.8 Hz, 1H), 7.68 (dd, J=9.4, 1.9 Hz, 1H), 7.85 (d, J=1.7 Hz, 1H), 7.92 (d, J=8.9 Hz, 1H), 8.34 (s, 1H), 8.39 (s, 1H), 8.43 (d, J=9.4 Hz, 1H); ^{13}C NMR (125 MHz, $CDCl_3$) δ 30.91, 30.95, 34.80, 35.40, 121.84, 121.88, 122.72, 125.08, 126.21, 126.60, 127.29, 128.22, 129.36, 130.10, 130.99, 132.06, 147.67, 149.44.

*4.4.3. (2,6-Di-tert-butyl-9-formylanthracene) (**6**).* To a mixture of **5** (100 mg, 0.29 mmol) in anhydrous DMF (3 mL) was added dropwise 1.6 M of *n*-BuLi (0.6 mL, 0.96 mol) at −78 °C and stirred for 2 h at room temperature. The mixture was poured onto water and extracted with CH_2Cl_2. The CH_2Cl_2 extract was washed with water and brine, dried ($MgSO_4$), filtered, and evaporated to give **6** (1.6 g, 45%) as pale-yellow solid. ^{1}H NMR (500 MHz, $CDCl_3$) δ 1.46 (s, 9H), 1.48 (s, 9H), 7.65 (dd, J=9.0, 1.8 Hz, 1H), 7.77 (dd, J=9.4, 1.9 Hz, 1H), 7.92 (d, J=1.7 Hz, 1H), 7.99 (d, J=8.9 Hz, 1H), 8.62 (s, 1H), 8.93 (d, J=9.4 Hz, 1H), 8.97 (s, 1H); ^{13}C NMR (125 MHz, $CDCl_3$) δ 30.83, 30.96, 34.79, 35.69, 117.92, 123.21, 123.47, 123.98, 125.05, 128.60, 128.79, 129.89, 131.04, 131.12, 132.11, 133.68, 134.59, 134.90, 136.57, 147.73, 151.66, 193.16.

*4.4.4. (2-(2,6-Di-tert-butylanthracen-9-yl)-1H-imidazo[4,5-f][1,10] phenanthroline) (**BAIP**).* **BAIP** was prepared by refluxing a mixture of phen-dione (1.33 g, 6.34 mmol), **7** (2.83 g, 8.86 mmol), ammonium acetate (9.70 g, 126.67 mmol), and glacial acetic acid (20 mL) for 1 h. After 30 min water (10 mL) is added and the mixture was cooled to 0 °C using an ice-bath and the mixture is stirred for 20 min. The mixture pH was adjusted to neutral by the dropwise addition of ammonia. The precipitate was filtered and dried over $MgSO_4$. Flash chromatography (CH_2Cl_2/methanol=10:1), after crystallization from CH_2Cl_2/*n*-hexane to give **BAIP** (1.6 g, 50%) as pale-yellow solid. IR (KBr, cm^{-1}), 1567, 1628, 3062, 2770, 2820, 3388. ^{1}H NMR (500 MHz, $CDCl_3$+DMSO-d_6) δ 1.10 (s, 9H), 1.25 (s, 9H), 7.36 (dd, J=9.3, 1.9 Hz, 1H), 7.42 (dd, J=8.9, 1.5 Hz, 1H), 7.50–7.56 (m, 2H), 7.69 (s, 1H), 7.71 (s, 1H), 7.76 (d, J=1.6 Hz, 1H), 7.84 (d, J=9.0 Hz, 1H), 8.36 (s, 1H), 8.63 (d, J=7.5 Hz, 1H), 8.91–8.96 (m, 3H); ^{13}C NMR (125 MHz, $CDCl_3$) δ 29.68, 29.85, 33.81, 34.07, 118.89, 118.97, 121.43, 121.51, 122.10, 122.12, 123.37, 124.06, 124.71, 125.29, 125.31, 127.05, 127.13, 127.33, 128.86, 129.15, 129.58, 129.61, 129.63, 129.84, 130.06, 142.44, 146.52, 146.67, 146.79, 147.73, 148.21. MS (EI, 70 eV) m/z 508 (M^+, base peak); HRMS (EI) calcd for $C_{35}H_{32}N_4^+$: 508.2621, found 508.2631.

*4.4.5. (2-(2,6-Di-tert-butylanthracen-9-yl)-1-methyl-1H-imidazo-[4,5-f][1,10] phenanthroline) (**1**).* To a stirred solution of **BAIP** (1.10 g, 2.16 mmol) in DMF (7 mL) at room temperature under nitrogen is added NaH (60%, 210 mg, 5.41 mmol) and the reaction mixture is stirred at room temperature. After 30 min, CH_3I (0.34 mL, 5.41 mmol) is added. After 18 h, water is added and the reaction mixture is extracted with ethyl acetate. The organic layer is washed with water and brine, dried over $MgSO_4$, and concentrated in vacuum. Flash chromatography (EtOAc/*n*-hexane=20:1) to give **1** (510 mg, 45%) as pale-yellow product. IR (KBr, cm^{-1}), 1371, 1567, 1628, 3062, 2770. ^{1}H NMR (500 MHz, $CDCl_3$) δ 1.26 (s, 9H), 1.43 (s, 9H), 3.95 (s, 3H), 7.44 (s, 1H), 7.50–7.53 (m, 2H), 7.61 (d, J=9.0 Hz, 1H), 7.72–7.75 (m, 2H), 7.98 (s, 1H), 8.05 (d, J=9.0 Hz, 1H), 8.60 (s, 1H), 8.85 (d, J=8.3 Hz, 1H), 9.14 (d, J=8.0 Hz, 1H), 9.22–9.24 (m, 2H); ^{13}C NMR (125 MHz, $CDCl_3$) δ 30.76, 30.86, 34.72, 34.90, 35.12, 118.91, 120.70, 121.51, 122.96, 123.41, 123.90, 124.72, 125.14, 125.76, 127.02, 128.51, 128.68, 129.30, 130.03, 130.87, 131.11, 131.74, 133.02, 136.24, 136.26, 139.91, 147.45, 147.83, 148.03, 149.79, 152.22, 154.32. MS (EI, 70 eV) m/z 522 (M^+, base peak); HRMS (EI) calcd for $C_{36}H_{34}N_4^+$: 522.2778, found 522.2783. EA calcd for C, 82.41; N, 10.68; H, 6.92. Found for C, 82.05; N, 10.63; H, 6.76.

*4.4.6. (2-(2,6-Di-tert-butylanthracen-9-yl)-1H-imidazo[4,5-f][1,10] phenanthroline-1-carbonitrile) (**2**).* To a stirred solution of **BAIP** (2.0 g, 3.94 mmol) in DMF (10 mL) at room temperature under nitrogen is added NaH (60%, 156 mg) and the reaction mixture stirred at room temperature. After 30 min, BrCN (464 mg, 4.25 mmol) is added. After 18 h, water is added and the reaction mixture is extracted with ethyl acetate. The organic layer is washed with water and brine, dried over $MgSO_4$, and concentrated in vacuum. Flash chromatography (EtOAc/*n*-hexane=20:1) was used to give **2** (1.4 g, 67%) as pale-yellow solid. IR (KBr, cm^{-1}), 740, 801, 1354, 1393, 2250, 2875, 2963. ^{1}H NMR (500 MHz, $CDCl_3$) δ 1.32 (s, 9H), 1.45 (s, 9H), 3.95 (s, 3H), 7.62–7.66 (m, 3H), 7.72 (d, J=9.2 Hz, 1H), 7.80–7.86 (m, 2H), 8.01 (d, J=0.9 Hz, 1H), 8.08 (d, J=9.0 Hz, 1H), 8.68 (s, 1H), 9.12–9.15 (m, 2H), 9.34 (d, J=4.3 Hz, 2H); ^{13}C NMR (125 MHz, $CDCl_3$) δ 30.73, 30.88, 34.95, 35.27, 105.47, 117.80, 118.19, 118.28, 123.31, 123.31, 123.47, 123.87, 124.16, 124.44, 125.36, 127.73, 127.89, 128.72, 129.89, 130.75, 130.98, 131.08, 131.38, 131.72, 136.06, 145.18, 145.33, 148.02, 150.20, 150.57, 152.76. MS (EI, 70 eV) m/z 533 (M^+, base peak); HRMS (EI) calcd for $C_{36}H_{31}N_5^+$: 533.2574, found 533.2581. EA calcd for C, 80.72; N, 13.07; H, 6.21. Found for C, 80.46; N, 12.87; H, 6.08.

Acknowledgements

We thank the Taipei Medical University and National Science Council for supporting this work. We thank Lu, J.-W., Instrumentation Center, National Taiwan University, for assistance in EA Analysis.

References and notes

1. Kido, J.; Kimura, M.; Nagai, K. *Science* **1995**, *267*, 1332–1334.
2. *Molecular Electronics: Science and Technology*; Aviram, A., Ratner, M. M., Eds.; New York Academy of Sciences: New York, NY, 1998; Vol. 852.
3. Tang, C. W.; Van Slyke, S. A. *Appl. Phys. Lett.* **1987**, *51*, 913–915.
4. Shi, J.; Tang, C. W. *Appl. Phys. Lett.* **1997**, *51*, 1665–1667.
5. Wakimoto, T.; Yonemoto, Y.; Funaki, J.; Tsuchida, M.; Murayama, R.; Nakada, H.; Matsumoto, H.; Yamamura, S.; Nomura, M. *Synth. Met.* **1997**, *91*, 15–19.
6. Murata, H.; Merritt, C. D.; Inada, H.; Shirota, Y.; Kafafi, Z. H. *Appl. Phys. Lett.* **1999**, *75*, 3252–3254.
7. Huang, W. S.; Lin, J. T.; Lin, H. C. *Org. Electron.* **2008**, *5*, 557–568.
8. Lai, M. Y.; Chen, C. H.; Huang, W. S.; Lin, J. T.; Ke, T. H.; Chen, L. Y.; Tsai, M. H.; Wu, C. C. *Angew. Chem., Int. Ed.* **2008**, *47*, 581–585.
9. Velusamy, M.; Justin Thomas, K. R.; Chen, C. H.; Lin, J. T.; Wen, Y. S.; Hsieh, W. T.; Lai, C. H.; Chou, P. T. *Dalton Trans.* **2007**, 3025–3034.
10. Shi, J.; Tang, C. W. *Appl. Phys. Lett.* **2002**, *80*, 3201–3203.
11. Naka, S.; Okada, H.; Onnagawa, H.; Tsutsui, T. *Appl. Phys. Lett.* **2000**, *76*, 197–199.
12. Yasuda, T.; Yamaguchi, Y.; Zou, D. C.; Tsutsui, T. *Jpn. J. Appl. Phys., Part 1* **2002**, *41*, 5626–5629.
13. Aziz, H.; Vamvounis, G.; Hu, N.X.; Popovic, Z.D.; Coggan, J.A. U.S. Pat. Appl. Publ. U.S. Patent 20,040,209,117, 2004.
14. Mondal, J. A.; Ramakrishna, G.; Singh, A. K.; Ghosh, H. N.; Mariappan, M.; Maiya, B. G.; Mukherjee, T.; Palit, D. K. *J. Phys. Chem. A* **2004**, *108*, 7843–7852.
15. Wang, R. Y.; Jia, W. L.; Aziz, H.; Vamvounis, G.; Wang, S.; Hu, N. X.; Popovic, Z. D.; Coggan, J. A. *Adv. Funct. Mater.* **2005**, *15*, 1483–1487.
16. Shi, L.; Li, B. *Eur. J. Inorg. Chem.* **2009**, *15*, 2294–2302.
17. Gao, F.; Zhao, Y.; Liang, W. Z. *J. Chem. Phys.* **2007**, *126*, 224509–224514.

18. He, A.; Zhong, C.; Huang, H.; Zhou, Y.; He, Y.; Zhang, H. *J. Lumin.* **2008**, *128*, 1291–1296.
19. Wu, J. Z.; Li, L.; Zeng, T. X.; Ji, L. N.; Zhou, J. Y.; Luo, T.; Li, R. H. *Polyhedron* **1997**, *16*, 103–107.
20. Natarajan, R.; Savitha, G.; Moorthy, J. N. *Cryst. Growth Des.* **2005**, *5*, 69–72.
21. Natarajan, R.; Savitha, G.; Dominiak, P.; Wozniak, K.; Moorthy, J. N. *Angew. Chem., Int. Ed.* **2005**, *44*, 2115–2119.
22. Moorthy, J. N.; Natarajan, R.; Venugopalan, P. *J. Org. Chem.* **2005**, *70*, 8568–8571.
23. Fu, P. P.; Harvey, R. G. *J. Org. Chem.* **1977**, *42*, 2407–2410.
24. Hutten, P. F. v.; Brouwer, H. J.; Krasnikov, V. V.; Ouali, L.; Stalmach, U.; Hadziioannou, G. *Synth. Met.* **1999**, *102*, 1443–1446.
25. Li, Y. Q.; Fung, M. K.; Xie, Z. Y.; Lee, S. T.; Hung, L. S.; Shi, J. M. *Adv. Mater. (Weinheim, Ger.)* **2002**, *14*, 1317–1321.
26. Shen, G. G.; Dunlap, Y. D.; Murata, H. H.; Kafafi, Z. H. *Appl. Phys. Lett.* **2001**, *79*, 2582–2584.